Proceedings World Geothermal Congress 2020+1
Reykjavik, Iceland, April - October 2021

Utah FORGE: Injection Test Interpretation

Mohammad J. Aljubran, Roland N. Horne and Mark D. Zoback

Stanford University School of Earth, Energy, and Environmental Sciences, Stanford, CA

aljubrmj@stanford.edu

Keywords: FORGE, EGS, Geomechanics, Injection

ABSTRACT

This study analyzed the in-situ stress regime of the Utah FORGE Well 58-32 based on a variety of measurements, including drilling reports, wireline logs, mud logs, drilling-induced wellbore failures, injection stimulation, and core samples. The focus of the study was Zone 1 (the deepest test interval). We concentrated on the analysis of injection stimulation tests to quantify the minimum horizontal stress (S_{hmin}). The overburden stress (S_v) gradient was first estimated as 1.13 psi/ft using density log measurements, rock cuttings, and shallow measurements of neighboring wells targeting the Roosevelt Hot Spring. Three stimulation injection techniques were investigated to estimate S_{hmin}: microfrac hydraulic fracturing tests, Diagnostic Fracture Injection Tests (DFIT) and Step-Rate Test (SRT). While the majority of microfac test cycles across Zone 1 were terminated prematurely, two cycles were interpretable. Assuming negligible friction at very low flow rates, these microfrac tests indicate a S_{hmin} gradient in the range of 0.71-0.76 psi/ft. Both the tangent and compliance interpretation methods were used to analyze the DFIT data. The tangent method resulted in very low S_{hmin} magnitudes. Given no clear evidence of fracture stiffness change after shut-in, the compliance method interpretation seems to be more appropriate as it indicates that the fracture walls closed immediately after shut-in such that the initial shut-in pressure (ISIP) should yield the best estimate of S_{hmin}. The ISIP readings were found to vary between 0.72 and 0.88 psi/ft depending on the fluid flow rate and cumulative volume associated with different cycles. Meanwhile, SRT data yielded an S_{hmin} gradient estimate of 0.79 psi/ft. Overall, the S_{hmin} gradient appears to be 0.75 +/- 0.4 psi/ft. Given that drilling-induced fractures indicate S_{Hmax} direction of N25°E, a stress polygon was constructed to constrain the S_{Hmax} gradient indicating normal/strike-slip regime at the greatest depth in Well 58-32. The large uncertainty in S_{Hmax} results from the marked effect of wellbore cooling on the occurrence of the drilling-induced hydraulic fractures.

1. INTRODUCTION

The Frontier Observatory for Research in Geothermal Energy (FORGE) is a field laboratory project launched by the US Department of Energy (DOE) in Utah to develop and evaluate technologies for sustainable Enhanced Geothermal Systems (EGS). It aims to support the adoption of EGS and demonstrate the state-of-the-art technology is sufficiently mature to tap hundreds of giga-wats of geothermal energy in high-temperature, low-permeability crystalline rock. In 2015, Phase 1 of the Utah FORGE project was launched with focus on site selection, conceptual geologic modelling, environmental management, and public outreach. As seen in Fig. 1, the Renewable Energy Corridor of Milford, Utah was selected to conduct the planned field experiments of Phase 2 (Moore et al. 2020).

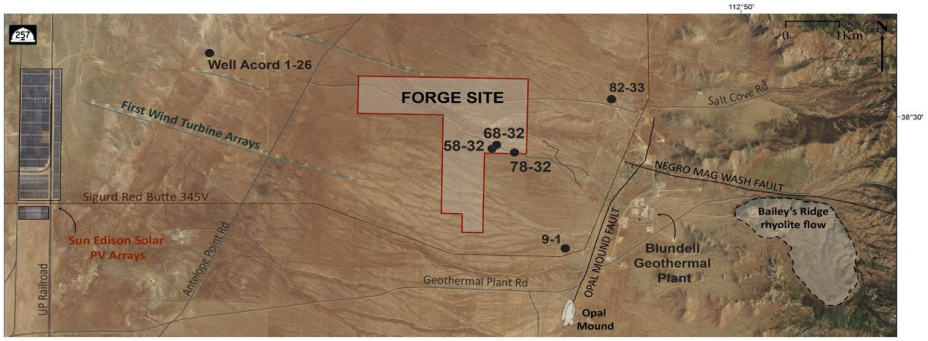

Figure 1: Map of the Renewable Energy Corridor of Milford, Utah which hosts the FORGE site along with other solar and wind projects. Well 58-32 was drilled and completed in 2018 to demonstrate the EGS potential in dry hot rock. Wells 68-32 and 78-32 were drilled next for seismic monitoring purposes (Moore et al. 2020).

While Phase 2A was intended to ensure the FORGE activities would not have presented environmentally incompatible site conditions, Phase 2B involved drilling the vertical Well 58-32, seen in Fig. 2, to a total depth of 7536-ft measured depth (MD) with 199°C (390°F), where low-permeability granitoid was encountered at 3175-ft MD. The objectives of Well 58-32 included the evaluation of drilling financial feasibility, rock and fluid properties, in-situ stress magnitudes and direction, and natural fracture networks. As seen in Table 1, four casing strings were run and cemented along Well 58-32 while 172 ft of openhole was left to allow for injection stimulation (Balamir et al. 2018). As part of the Phase 2B plan, a full suite of geophysical logs (gamma, density, neutron, sonic, and others), pressure/temperature surveys, Formation Micro Imager (FMI), and coring were collected across the 8-3/8-in openhole section before running and cementing the 7-in casing. In addition, injection stimulation was conducted across the uncased 172-ft openhole to assess the least principal stress and permeability, and evaluate natural and drilling-induced fractures. In 2019, to further understand the in-situ stresses at the FORGE site, Phase 2C involved additional injection stimulation testing was conducted across three zones: 172-ft openhole (Zone 1), perforated casing between 6964 and 6974-ft MD (Zone 2), and perforated casing between 6565 and 6575-

ft MD (Zone 3). Zone 2 was selected as it contained an abundance of preexisting fractures that were anticipated to be critically stressed while Zone 3 was selected as FMI log analysis showed it would be difficult to break down (Xing et al. 2020).

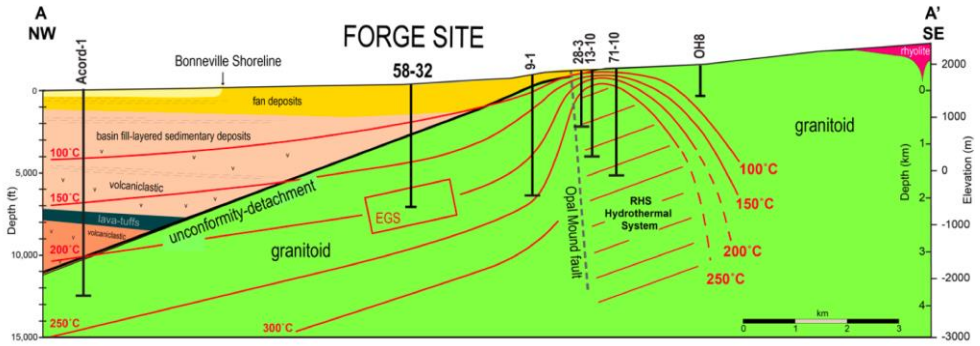

Figure 2: Cross-section of the FORGE site, showing the deep test Well 58-32 and the opal Mound fault which separate the FORGE EGS target from the Roosevelt Hot Spring (RHS) (Energy and Geoscience Institute at the University of Utah 2019).

Table 1: Well 58-32 Casing Design		
Openhole OD, in	Casing OD, in	Shoe Depth, ft MD
40	20	84
17-1/2	13-3/8	337.5
12-1/4	9-5/8	2172
8-3/8	7	7364
8-3/8	-	7536

Over the past two years, the FORGE team analyzed and interpreted the collected data and summarized their findings in the Phase 2C Topical Report (Energy and Geoscience Institute at the University of Utah 2019). However, the analysis of the injection stimulation was inconclusive in that wide ranges of principal stress magnitudes were reported based on different data and interpretation methods. Hence, this study aimed to review common injection stimulation interpretation methods, and analyze the recently collected Utah FORGE data[1] across Zone 1 (openhole).

2. METHODOLOGIES

This section will review the different methods which were used (or evaluated) in estimating the direction and absolute magnitudes of the overburden stress, minimum horizontal principal stress, and maximum horizontal principal stress. Meanwhile, pore pressure was measured directly in Well 58-32 and found to be hydrostatic, 0.433 psi/ft.

2.1 Overburden Stress (S_v)

Assuming that S_v is a principal stress, it can be estimated using density log measurements. In onshore areas, S_v is equivalent to the integral of rock density over depth (Zoback 2007). Note that true vertical depth (TVD) must be used to calculate this cumulative rock density. Well 58-32 experienced deviation from vertical across multiple depths; hence, correction of MD to TVD is required to acquire an accurate estimate of S_v. The average tangential method, seen in Eq. 1, is used to approximate TVD between any MD and θ measurements.

$$TVD_i = TVD_{i-1} + (MD_i - MD_{i-1}) \cdot Cos\left(\frac{\theta_i - \theta_{i-1}}{2}\right) \quad (1)$$

2.2 Minimum Horizontal Stress (S_{hmin})

Multiple techniques have been proposed over the past few decades to measure the relative and/or absolute magnitudes of S_{hmin}. Most commonly, Earth focal plane mechanisms interpretation is used to estimate the relative magnitudes of the in-situ stresses, which allows for identifying the stress regime. Meanwhile, minifracs, leak-off tests, diagnostic fracture injection testing (DFIT), and step-rate tests (SRT) are used nowadays to estimate the absolute magnitude of S_{hmin}. This study evaluated the injection stimulation tests to allow for an estimate of the absolute magnitude of S_{hmin}, which has further applications when available, such as constraining the maximum horizontal stress magnitude. In addition, analysis of drilling-induced tensile failure and breakouts was accounted for in this work.

2.2.1 Minifrac Tests

A minifrac extended leakoff test is an injection diagnostic procedure that aims to measure the magnitude of the least principal stress. A constant pumping rate into a shut-in wellbore (closed system) results in a linearly increasing pressure over time. At a point with

[1] Utah FORGE data: https://dx.doi.org/10.15121/1578287

sufficiently high pressure, the fluid leaks into the formation due to the formation of a hydraulic fracture resulting in pressure departure from the linear trend (Zoback 2007). If conducted properly, minifrac tests can provide good estimates of S_{hmin}.

2.2.2 DFIT Interpretation

DFIT test interpretation for the determination of S_{hmin} has been controversial in heterogeneous and low permeability reservoirs (Zoback and Kohli 2019). The literature shows two major approaches in this area: tangent (or holistic) method (Barree et al. 2007; Craig et al. 2006) and compliance method (McClure et al. 2019; Wang and Sharma 2018; Jung et al. 2016).

The conventional tangent method was originally proposed by Barree et al. (2007) based on the G-function. The G-function, a dimensionless monotonic transformation of the shut-in time, was first defined by Nolte (1979). He made several reasonable assumptions, including constant fracture height, quasielastic fracture propagation across the rock matrix, symmetric fracture wings, no slip on bedding planes, power-law fluid injection, fracture propagation stops immediately after pumping stops, and fracture closes freely without proppant support. Given these assumptions, a g-function (related, but different from G-function) is defined to be linearly proportional with the cumulative injection fluid leakoff before shut-in. Similarly, the cumulative leakoff is linearly proportional to the G-function after shut-in (Castillo 1987; Gulrajani and Nolte 2000). Subsequently, the tangent method relies on the analysis of the $G\ dP/dG$ curve along G-Time which, by construction, is only valid after shut-in time. The tangent method assumes that a straight line reflects Carter leakoff and a concave-downward inflection reflects S_{hmin}. Barree et al. (2007) summarized the tangent interpretation method as drawing a tangent line from the origin to the $G\ dP/dG$ where S_{hmin} is the point where this plot starts to curve down. They argue that most of the other behavior can be explained by fracture tip extension, pressure-dependent leakoff, fracture height recession, and /or closure of transverse fractures.

McClure et al. (2014; 2016; 2019) argued that the so-called ideal $G\ dP/dG$ curve is rarely seen in low-permeability formation, where it rather curves upwards during injection in the majority of cases. Hence, they proposed the compliance method which is based on the observation that a fracture retains a finite aperture upon mechanical closure as asperities come into contact. Jung et al. (2016) used CFRAC (Complex Fracturing ReseArch Code), developed by McClure and Horne (2013), to contrast the tangent and compliance methods across a variety of low-permeability scenarios, including two-dimensional and three-dimensional cases. In low-permeability scenarios, they showed that the tangent method severely underestimates S_{hmin} with 50 MPa (7250 psi) while the compliance interpretation yields 55 MPa (7975 psi) which is closer to the instantaneous shut-in pressure (ISIP). Zoback and Kohli (2019) argue that the tangent method tends to overestimate the net pressure (typically order of 1000's psi in net pressure) which results in unrealistic fracture geometry while the compliance method (typically order of 100's psi in net pressure) is physically reasonable. In addition, using ISIP to estimate S_{hmin} in igneous rocks, i.e. Utah FORGE granitoid rock, is backed with theoretical and experimental literature (Hickman and Zoback 1983; Hickman and Davatzes 2010).

2.2.3 Step-Rate Test (SRT) Interpretation

SRT has been in use for decades to determine the formation/fracture opening pressure, hence S_{hmin}. Given a stable hydrostatic column, SRT is conducted as a series of constant-rate steps that are increased in a stepwise manner, such that all steps have equal time length (Zoback and Haimson 1982; Singh et al. 1987). Prior to opening a hydraulic fracture and assuming steady-state Darcy flow into the well, the slope is defined by diffusion into the formation and/or closed hydraulic fracture (Zoback 2007). Note that viscous fluid frictional losses could also be subtracted to reflect the actual downhole pressure; however, they are less significant at lower pumping rates where the hydraulic fracture opening pressure is picked, so they will be neglected in this study.

2.3 Maximum Horizontal Stress (S_{Hmax})

FMI logging of Well 58-32 revealed more than 2000 natural fractures and 356 drilling-induced fractures, but no breakouts were observed (Moore et al. 2020). Using this knowledge, log and core measurements, S_{hmin} estimate from injection stimulation, this study will constrain the range of S_{Hmax} using a stress polygon as proposed and detailed by Zoback (2007). Three constraints were considered in this analysis: fault equilibrium, presence of tensile failures, and absence of breakouts, seen in Eqs. 2-4, respectively.

$$S_1 \leq \left[\sqrt{(\mu^2+1)}+\mu\right]^2 \left(S_3 - P_p\right) + P_p \tag{2}$$

$$S_{Hmax} \geq 3S_{hmin} - 2P_p - \Delta P - T_0 \ - \sigma^{\Delta T} \tag{3}$$

$$S_{Hmax} \leq \frac{\left(C_o+2P_p+\Delta P+\sigma^{\Delta T}\right)-S_{hmin}\left(1+2Cos(\pi-w_{bo})\right)}{1-2Cos(\pi-w_{bo})} \tag{4}$$

3. RESULTS AND DISCUSSION

Based on the aforementioned methodologies, this section will present analyze the FORGE data across Zone 1 (openhole) and contrast the findings with those communicated in the most recent publications by the FORGE team, who reported S_v, S_{hmin}, and S_{Hmax} gradients of 1.13, 0.62, and 0.77 psi/ft, respectively.

3.1 Overburden Stress (S_v)

density log measurements were conducted across the 8-3/4-in hole section, starting just below the 9-5/8-in casing shoe at 2172-ft MD. Meanwhile, density at shallower depths was estimated based on rock cuttings and other previous density measurements from neighboring wells. Using Eq. 1, TVD is estimated using depth and inclination measurements while overburden was calculated as the density integral. This resulted in S_v gradient of 1.13 psi/ft, closely matching the FORGE team findings. Meanwhile, pore pressure was estimated to be hydrostatic based on direct measurements at Well 58-32.

3.2 Minimum Horizontal Stress (S_{hmin})

Interpretations of minifrac, DFIT and SRT injection stimulation tests are demonstrated in this section and contrasted with that done by the FORGE team. Note that this analysis will focus on Zone 1 (openhole) injection stimulation measurements in both 2017 and 2019 as seen in Fig. 3. These injection stimulation test records included other operations as well (i.e. setting packer, pressure testing equipment, etc.) along with multiple cycles of minifrac and DFIT. Meanwhile, some cycles were terminated before reaching the fracture propagation pressure, hence they are deemed incomplete and not considered in the estimation of S_{hmin}. It is important to notice that no breakdown was observed throughout these tests. Also, note that all gradient calculations were performed based on fracture opening depth of 7400-ft TVD, just below the 7-in casing shoe.

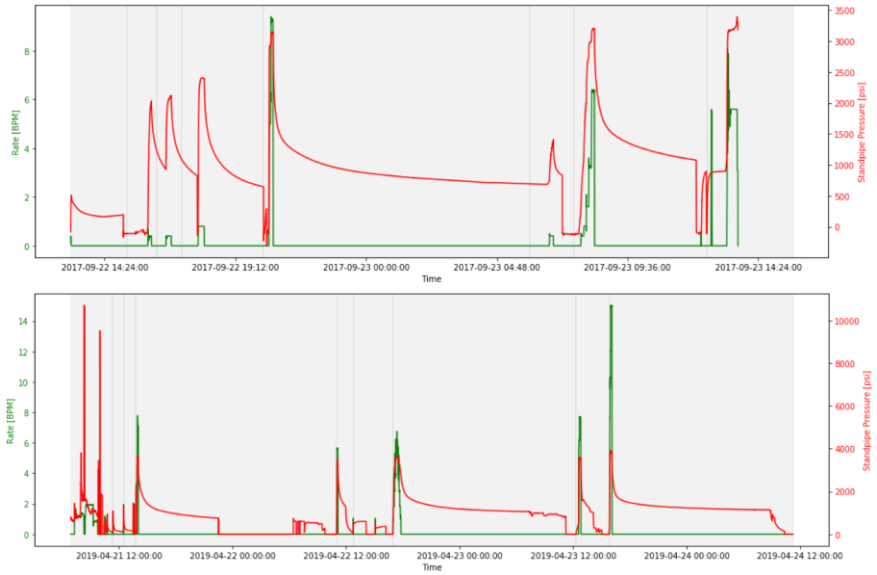

Figure 3: 2017 (top) and 2019 (bottom) injection stimulation tests across Zone 1 (openhole) of Well 58-32. These plots show other operations (setting packer, pressure testing equipment, etc.) besides minifrac, DFIT and SRT tests. Grey bars indicate different operations and/or minifrac/DFIT cycles.

2017 and 2019 witnessed multiple attempts to perform minifrac tests across Zone 1; however, the majority of these tests were either incomplete or inconclusive. After inspecting and analyzing these tests, we found that only cycles 3 and 4 of 2017 could yield useful estimates of S_{hmin}. Note that no breakdown was observed in these tests, which could indicate the presence of preexisting fractures. Given that cycles 3 and 4 of 2017 were conducted with low-viscosity brine at very low pumping rates (negligible frictional losses), S_{hmin} is estimated using the surface pumping pressure at the pressure versus flow rate plateau. Seen in Fig. 4, the pumping pressure plateaus at approximately 2100 and 2400 psi in cycles 3 and 4, respectively. Adding the hydrostatic column translates to 0.71, and 0.76 psi/ft as the S_{hmin} gradient.

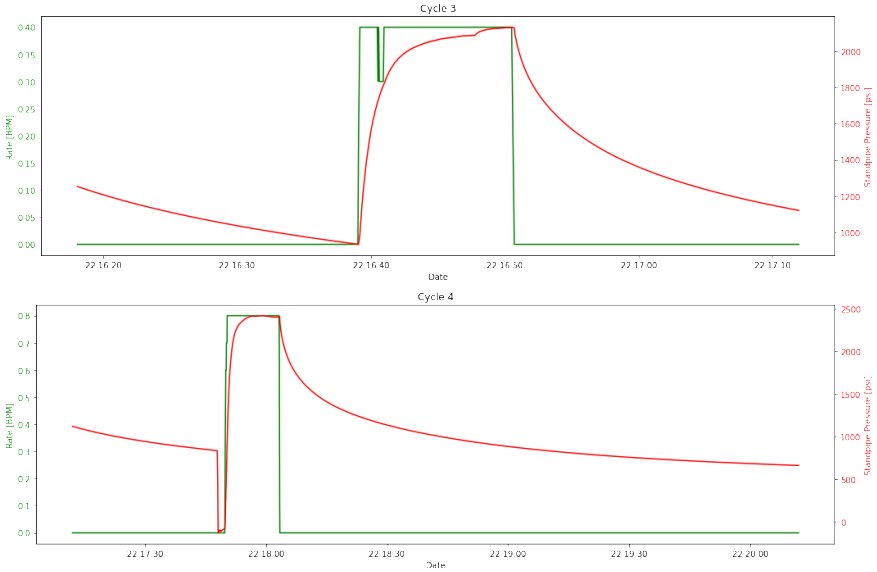

Figure 4: Cycles 3 (top) and 4 (bottom) of the 2017 injection microfrac tests. While no breakdown is observed, the pumping pressure plateau is used to estimate S_{hmin}.

Following the approach proposed by Barree et al. (2007), Figs. 5 and 6 show the tangent method interpretation of two DFIT injection cycles conducted in 2017. Barree et al. (2007) interprets such curves as 'pressure-dependent leakoff' and/or 'fracture tip-extension'. Drawing a tangent to the $G\ dP/dG$ plot as it curves downward, starting at G-time of zero and accounting for the mud hydrostatic pressure, the S_{hmin} would take magnitudes of 4204 and 5204 psi based on the top and bottom cycles, respectively, of Fig. 5. At 7400-ft TVD, these translate to S_{hmin} gradients of 0.56 and 0.70 psi/ft. Similarly, Fig. 6 shows the tangent method interpretation of two DFIT injection cycles conducted in 2019 across Zone 1, resulting in gradients of 0.73 and 0.67 psi/ft. It is intriguing to observe that all of these tangent method interpretations indicate fracture net pressure magnitudes of 1000 to 2000 psi, which is too high and would yield unrealistic fracture geometries (Zoback and Kohli 2019).

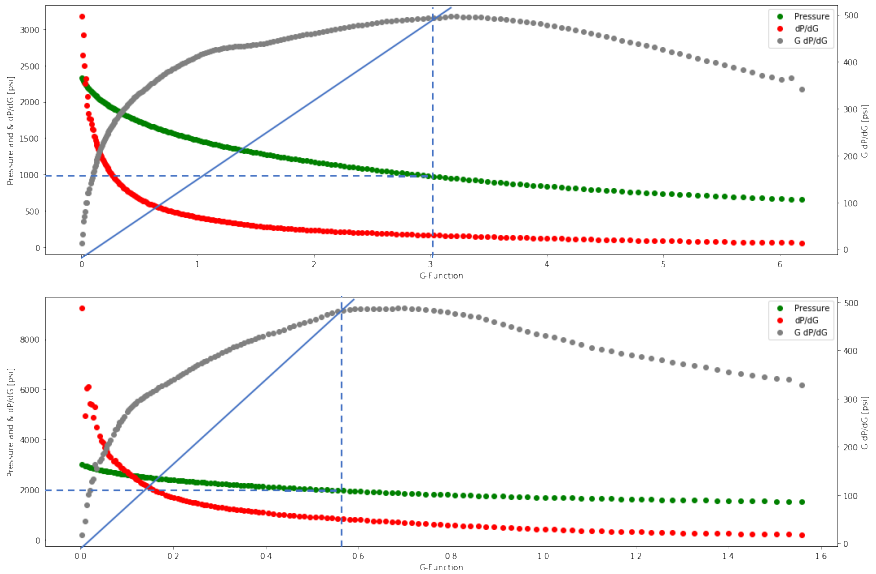

Figure 5: 2017 DFIT across Zone 1 where G-Function is used to demonstrate the tangent method interpretation across two different cycles as proposed by Barree et al. (2007). The blue line indicates the tangent to the $G\ dP/dG$ curve which indicates S_{hmin} magnitudes of 4204 and 5204 psi on the top and bottom cycles, respectively.

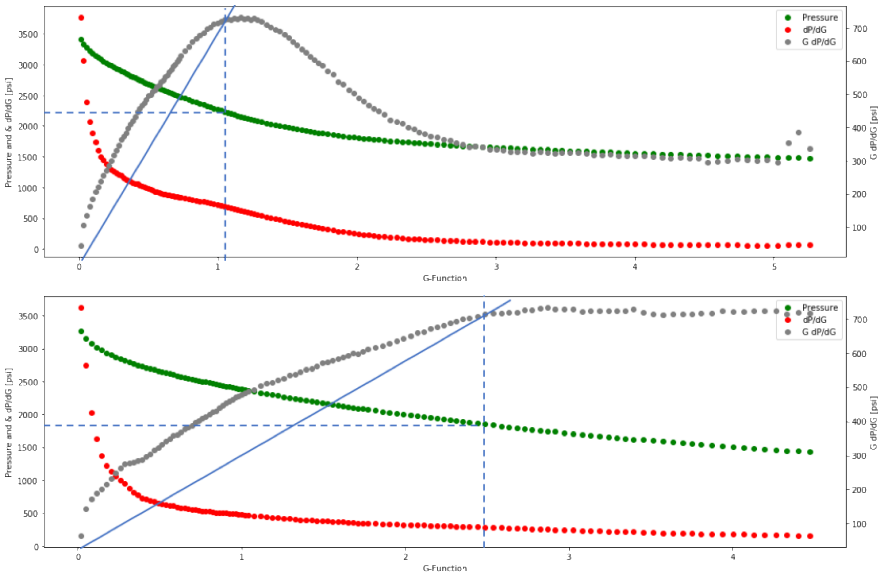

Figure 6: 2019 DFIT across Zone 1 where G-Function is used to demonstrate the tangent method interpretation across two different cycles as proposed by Barree et al. (2007). The blue line indicates the tangent to the $G\ dP/dG$ curve which indicates S_{hmin} magnitudes of 5454 and 5004 psi on the top and bottom cycles, respectively.

Meanwhile, the compliance method proposed by McClure et al. (2019) suggests that the minimum of the dP/dG curve is where S_{hmin} should be measured. However, Figs. 5-6 indicate that the dP/dG curve is decreasing monotonically without clear inflection points. McClure et al. (2019) analyzed a similar case, DFIT in the Middle Bakken, and described it to be hardly interpretable. They attributed such G-Time plot behavior to one or more of the following phenomena:

a. If significant fluid volume was pumped into the formation prior to DFIT, such that DFIT involves reinjection into hydraulic fractures

b. If injection is done directly into a highly conductive fracture

c. If hydraulic fracture intersects a highly conductive natural fracture

d. If matrix permeability is significantly high relative to the fluid viscosity (>0.01-0.1 md/cp)

e. If near-wellbore pressure drop is very severe, masking far-field fracture pressure transient

Observing FMI logs before and after DFIT, phenomena ‘a’, ‘b’, and ‘c’ are possible (‘d’ is eliminated because granite is a low-permeability rock while ‘e’ is also eliminated because Well 58-32 is vertical and less likely to experience significant near-wellbore pressure drops). FMI log measurements, seen in Fig. 7, confirmed that both drilling-induced and natural fractures preexisted prior to DFIT. In addition, the drilling-induced fractures increased in aperture, indicating that they reopened during DFIT which explains the absence of a breakdown record.

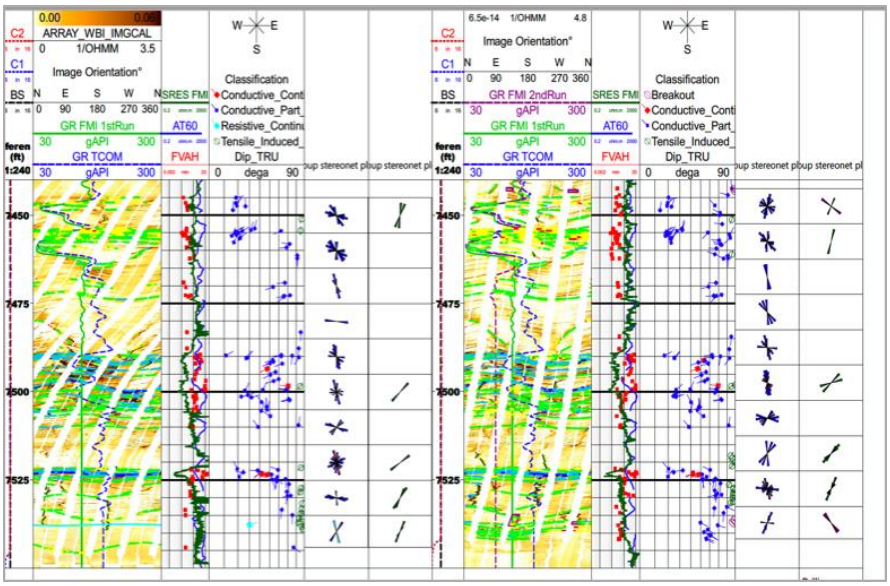

Figure 7: FMI log before (left) and after (right) injection stimulation. The FORGE team interpretation indicates many conductive natural and drilling-induced hydraulic fractures existed prior to DFIT. In addition, some of these fractures grew in aperture after DFIT. Meanwhile, breakouts were not present during drilling and were barely observed after DFIT (the indicated breakout interpretations are found very uncertain after examining the full FMI log).

In these cases, McClure et al. (2019) indicate that ISIP would be the best estimate of S_{hmin}, which is supported by other theoretical and experimental literature (Hickman and Zoback 1983; Hickman and Davatzes 2010). Fig. 8 shows cycle 5 of the 2017 and cycle 8 of the 2019 injection stimulation for illustration, where ISIP is picked as 2922 and 3322 psi, respectively. These interpretations yield S_{hmin} gradients of 0.828 and 0.882 psi/ft, respectively. Interpreting the other DFIT cycles across Zone 1, S_{hmin} gradients range between 0.72-0.88 psi/ft, seen in Fig. 9, which is a significantly wide range. It is noticeable that these interpretations show an increasing trend of ISIP with respect to the cumulative volume pumped (and also the volume pumped per cycle). McClure et al. (2019) attribute similar behaviors to preexisting fractures. There is no ‘toughness’ to overcome in the case of a preexisting fracture, so it opens just enough to conduct fluid. After shut-in, the fracture walls come into contact immediately while fluid continues to flow outward into the fracture network, hence ISIP retains higher magnitudes.

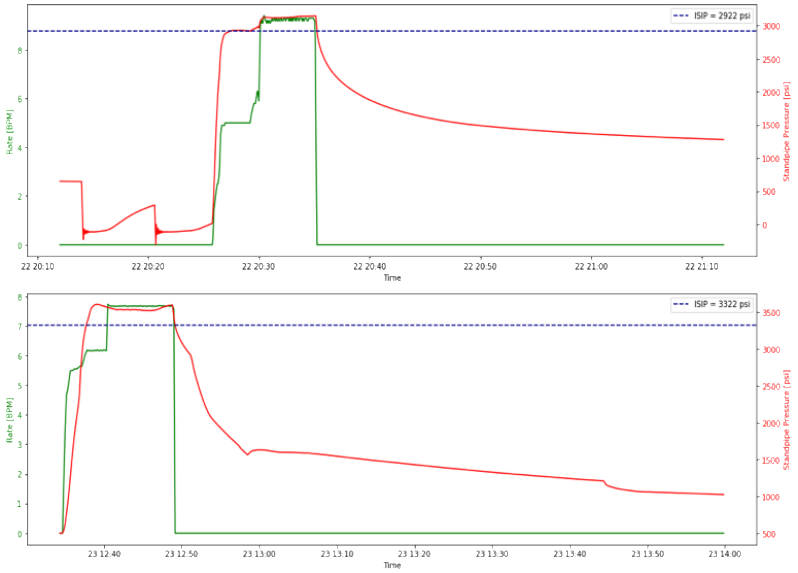

Figure 8: Cycle 5 of the 2017 (top) and cycle 8 of the 2019 (bottom) injection stimulation tests across Zone 1 (openhole) of Well 58-32. These plots show ISIP values of 2922 and 3322 psi, respectively.

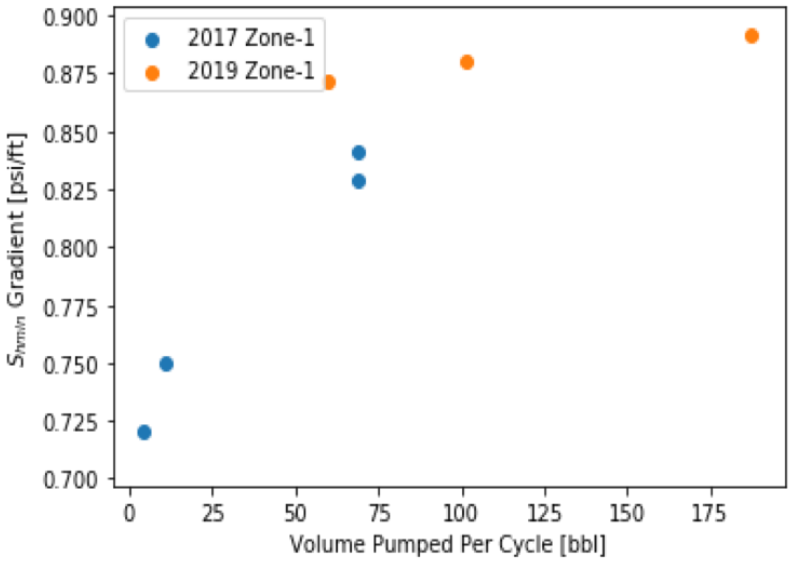

Figure 9: Illustration in the inconsistence of the ISIP readings and rather dependence on the volume pumped per cycle. This is attributed to immediate fracture wall contact after shut-in, hence DFIT readings are more difficult to interpret using ISIP. Note that this plot should not be used to interpret S_{hmin}, but rather SRT plots are used to account for the relationship between pumping pressure and flow rate, and capture fracture reopening pressure.

SRT data, seen in Fig. 10, is less dependent on this phenomenon as it is based on increasing pressures (fracture wall opening), rather than decreasing pressures (fracture wall closing). Fig. 11 shows the interpretation of the 2017 and 2019 data, yielding closely matching S_{hmin} gradients of 0.784 and 0.798 psi/ft, respectively. Hence, a value of 0.79 psi/ft will be considered the most reliable. Meanwhile, FORGE team publications indicated a range of 0.55-0.85 psi/ft using different methods of interpretations and ultimately used 0.62 psi/ft as their final interpretation for the S_{hmin} gradient.

Figure 10: 2017 (top) 2019 (bottom) SRT injection stimulation tests across Zone 1 (openhole) of Well 58-32.

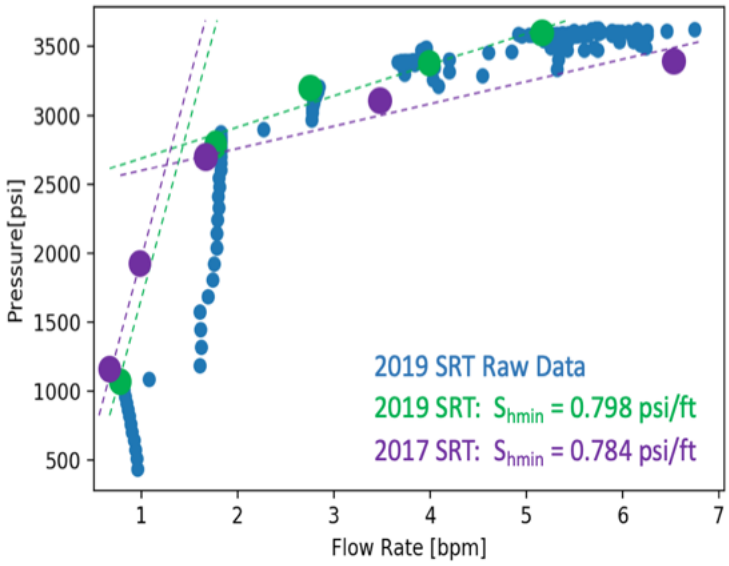

Figure 11: Interpretation of 2017 (top) 2019 (bottom) SRT injection stimulation tests across Zone 1 (openhole) of Well 58-32, yielding S_{hmin} gradients of 0.784 and 0.798 psi/ft, respectively.

3.3 Maximum Horizontal Stress (S_{Hmax})

As proposed by Zoback (2007), Eqs. 2-4 allow us to constrain S_{Hmax} when knowledge of S_v, S_{hmin}, and other geological properties are available. Based on core laboratory experiments, wireline logging, mud logging, observed wellbore tensile and compressive failures, and reservoir injection stimulation, the FORGE team published their best estimates of different properties required to construct the stress polygon and constrain S_{Hmax} (Moore et al. 2020, Nadimi et al. 2019; Kamali et al. 2020). Note that Mohr-Coulomb failure criterion is used in this analysis (Vermylen 2011).

Seen in Fig. 7, FMI logging shows clear records of drilling-induced tensile failure, indicating that the direction of S_{Hmax} is N25°E. Meanwhile, no breakouts were observed during drilling. The borehole across the openhole does not show any significant deviation, so it will be considered vertical. Based on drilling reports, mud overbalance was less than 500 psi overall, with a gradient of around 0.04 psi/ft across the zone of interest. Biot coefficient, sliding friction, internal friction, Poisson's ratio, Young's modulus, unconfined compressive strength, tensile strength, and linear thermal expansion coefficient were reported as 1.0, 0.82, 0.6, 0.25, 6.5×10^6 psi, 25380 psi, 0 psi, and 2.0×10^{-6} 1/°F, respectively. Across the depth of interest, mud loggers recorded mud flow-in and flow-out temperatures of 121 and 139° F compared to the bottomhole granitoid temperature of 390° F. To further observe the cooling effect, the stress polygon is constructed for a range of ΔT values (0, -125, and -251°F).

As seen in Fig. 12, the software GMI SFIB was used to generate stress polygons across the aforementioned values of ΔT. Note that increasing the cooling effect (magnitude of ΔT) increases the likelihood of tensile failure, hence the lower bound of S_{Hmax} decreases which results in a wider range of possibilities. At ΔT magnitudes closer to -250°F, the stress polygon yields inconclusive results in

constraining S_{Hmax}. Based on this analysis, we conclude that a normal/strike-slip regime is most likely in this region with $S_{Hmax} \approx S_v$. It is noteworthy that Lund-Snee and Zoback (2020) recently constructed a relative stress magnitude map of the United States, indicating the possibility of both normal and strike-slip regime across the Utah FORGE site.

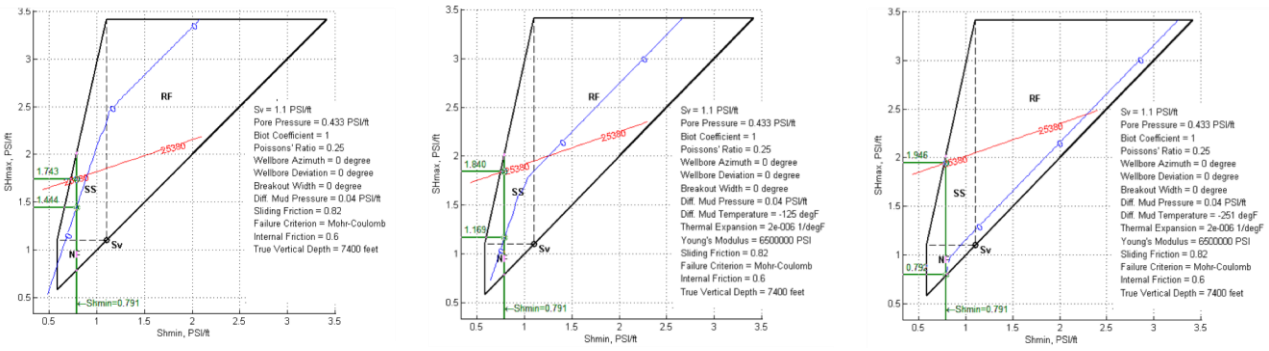

Figure 12: Stress polygon based on the analysis of Well 58-32 Zone 1. Note that both the tensile failure (blue) and breakout (red) limits shift in the left, center, and right polygons due to the different cooling effect with ΔT values of 0, -125, and -251°F, respectively.

Furthermore, an analysis of slip on preexisting fracture is analyzed using the Mohr-Coulomb failure criterion. Following the convention proposed by Zoback and Lund-Snee (2018), this study represents the Mohr circle using normal stress rather than effective normal stress on the x-axis. Fig. 13 shows the results at different values of pressure in the pores due to increasing mud overbalance. Note that the failure line has slope of 0.82 (sliding friction) and it moves to the right, starting at pore pressure of 3204 psi, as mud overbalance increases. Fig. 13 shows two cases: no pressure is applied to the reservoir (top), and nearly 2000 psi additional pressure reaching the pore space (bottom) due to injection stimulation. It is evident that some fractures (red) were mechanically and hydraulically active under the injection stimulation testing conditions, which further justifies the absence of breakdown as observed during injection stimulation.

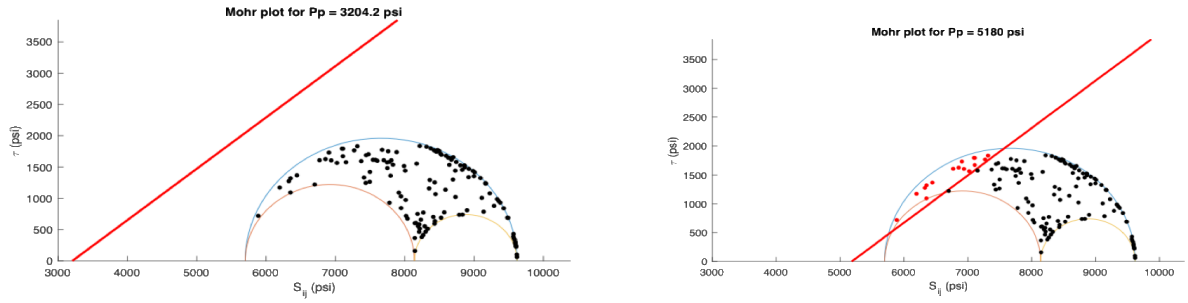

Figure 13: Mohr circle plot based on zero (left) and nearly 2000 psi (right) net pore pressure. This aims to simulate the effective increase of pore pressure during DFIT operations.

CONCLUSION

This study analyzed the in-situ stress regime of the Utah FORGE Well 58-32 based on a variety of measurements, including drilling reports, wireline logs, mud logs, drilling-induced wellbore failures, injection stimulation, and core samples with focus on Zone 1. Three stimulation injection techniques were investigated to estimate S_{hmin}: microfrac hydraulic fracturing tests, Diagnostic Fracture Injection Tests (DFIT) and a Step-Rate Test (SRT). The tangent method resulted in unrealistically low S_{hmin} estimates. Given no clear evidence of fracture stiffness change after shut-in, the compliance method interpretation seems to be more appropriate as it indicates that the fracture walls closed immediately after shut-in such that the initial shut-in pressure (ISIP) should yield the best estimate of S_{hmin}. The ISIP readings were found to vary between 0.72 and 0.88 psi/ft depending on the fluid flow rate and cumulative volume associated with different cycles. The SRT yielded an estimate S_{hmin} gradient of 0.79 psi/ft. Overall, the S_{hmin} gradient appears to be 0.75 +/- 0.4 psi/ft. Given that drilling-induced fractures indicate S_{Hmax} direction of N25°E, a stress polygon was constructed to constrain the S_{Hmax} showing that a normal/strike-slip regime is most likely at the greatest depth in Well 58-32. Note that these findings do not fully agree with the normal faulting stress regime published by the FORGE team (S_v, S_{hmin}, and S_{Hmax} gradients of 1.13, 0.62, and 0.77 psi/ft, respectively).

NOMENCLATURE

ρ	*Density*	S_1	*Maximum Principal Stress*
μ	*Coefficient of Sliding Friction*	S_2	*Intermediate Principal Stress*
$\sigma^{\Delta T}$	*Thermal Stress*	S_3	*Minimum Principal Stress*
ΔP	*Difference of Mud and Formation Pressure*	S_{Hmax}	*Maximum Horizontal Stress*
A	*Fracture Surface Area*	S_{hmin}	*Minimum Horizontal Stress*
A_Φ	*Relative Stress Magnitude*	S_v	*Overburden Stress*
C_0	*Unconfined Compressive Strength*	T	*Temperature*
C_L	*Leakoff Coefficient*	t_s	*Shut-in Time*
g	*Gravitational Constant (9.81 m/s^2)*	TVD	*True Vertical Depth*
$g(\Delta t)$	*g-function of Δt*	V_L	*Cumulative Leakoff Volume Before Shut-in*
$G(\Delta t)$	*G-function of Δt*	V_{LS}	*Cumulative Leakoff Volume After Shut-in*
MD	*Measured Depth*	w_{bo}	*Breakout Width*
P	*Pressure*	z	*Depth*
P_p	*Pore Pressure*		

REFERENCES

Allis, R., Gwynn, M., Harwick, C, et al. 2018. Thermal Characteristics of the FORGE site, Milford, Utah. *Transactions, Geothermal Resources Council* **42**.

Balamir, O., Rivas, E., Rickard, W., et al. 2018. Utah FORGE Reservoir: Drilling Results of Deep Characterization and Monitoring Well 58-32. Paper Presented at the 43rd Workshop on Geothermal Reservoir Engineering at Stanford, California, February 10-12.

Barree, R., Barree, V., and Craig, D. 2007. Holistic Fracture Diagnostics. *SPE Rocky Oil & Gas Technology Symposium*. https://doi.org/10.2118/107877-MS.

Castillo, J. 1987. Modified Fracture Pressure Decline Analysis Including Pressure-Dependent Leakoff. SPE-16417-MS Paper Presented at the SPE/DOE Joint Symposium on Low Permeability Reservoirs, Denver, Colorado, 18-19 May. https://doi.org/10.2118/16417-MS.

Craig, D. and Blasingame, T. 2006. Application of a New Fracture-Injection/Falloff Model Accounting for Propagating, Dilated, and Closing Hydraulic Fractures. SPE-100578-MS Paper Presented at the SPE Gas Technology Symposium, Calgary, Canada, 15-17 May. https://doi.org/10.2118/100578-MS.

Energy and Geoscience Institute at the University of Utah. 2018. Utah FORGE: Final Topical Report 2018 [data set]. Retrieved from http://gdr.openei.org/submissions/1038.

Energy and Geoscience Institute at the University of Utah. 2019. Utah FORGE: Phase 2C Topical Report [data set]. Retrieved from http://gdr.openei.org/submissions/1187.

Gulrajani, S. and Nolte, K. 2000. Fracture Evaluation Using Pressure Diagnostics. In Economides, M. and Nolte, K. (eds), *Reservoir Simulation.* New York: Wiley.

Hickman, S. and Davatzes, N. 2010. In-Situ Stress and Fracture Characterization for Planning of an EGS Stimulation in the Desert Peak Geothermal Field, Nevada. Paper Presented at the 35th Workshop on Geothermal Reservoir Engineering at Stanford, California, February 1-3.

Hickman, S. and Zoback M. 1983. The Interpretation of Hydraulic Fracturing Pressure-Time Data for In-Situ Stress Determination. Paper Presented at the Hydraulic Fracturing Stress Measurements Workshop.

Jung, H., Sharma, M., Cramer, D., et al. 2016. Re-examining Interpretations of Non-ideal Behavior during Diagnostic Fracture Injection Tests. *Journal of Petroleum Science and Engineering* **145**: 114-136.

Kamali, A., Ghassemi, A., McLennan, J., et al. 2020. Analysis of FORGE DFIT Considering Hydraulic and Natural Fracture Interactions. Paper Presented at the 45th Workshop on Geothermal Reservoir Engineering at Stanford, California, February 10-12.

Lund-Snee, J. and Zoback, M. 2020. Multiscale Variations of the Crustal Stress Field Throughout North America. *Nature Communications* **11**. https://doi.org/10.1038/s41467-020-15841-5

McClure, M. 2017. The Spurious Deflection on Log-Log Superposition-Time Derivative Plots of Diagnostic Fracture-Injection Tests. *SPE Reservoir Evaluation & Engineering* **22**(4). https://doi.org/10.2118/186098-PA.

McClure, M. and Horne, R. 2013. Discrete Fracture Network Modelling of Hydraulic Stimulation: Coupling Flow and Geomechanics. Springer: New York. https://doi.org/10.1007/978-3-319-00383-2.

McClure, M., Bammidi, V., Cipolla, C., et al. 2019. A Collaborative Study on DFIT Interpretation: Integrating Modeling, Field Data, and Analytical Techniques. URTEC-2019-123-MS Paper Presented at the SPE/AAPG/SEG Unconventional Resources Technology Conference, Denver, Colorado, 22-24 July. https://doi.org/10.15530/urtec-2019-123.

McClure, M., Blyton, C., Jung, H., et al. 2014. The Effect of Changing Fracture Compliance on Pressure Transient Behavior During diagnostic Fracture Injection Tests. SPE-170956-MS Paper Presented at the SPE Annual Technical Conference and Exhibition (ATCE) in Amsterdam, The Netherlands, 27-29 October. https://doi.org/10.2118/170956-MS.

McClure, M., Jung, H., Cramer, D., et al. 2016. The Fracture-Compliance Method for Picking Closure Pressure from Diagnostic Fracture-Injection Tests. *SPE Journal* **4**(21): 1321-1339. http://dx.doi.org/10.2118/179725-PA.

Moore, J., McLennan, J., Allis, R., et al. 2020. The Utah Frontier Observatory for Research in Geothermal Energy (FORGE): A Laboratory for Characterizing, Creating and Sustaining Enhanced Geothermal Systems. Paper Presented at the 45th Workshop on Geothermal Reservoir Engineering at Stanford, California, February 10-12.

Nadimi, S., Forbes, B., Moore, J., et al. 2019. Effect of Natural Fractures on Determining Closure Pressure. *Journal of Petroleum Exploration and Production Technology* **10**: 711-728. https://doi.org/10.1007/s13202-019-00769-4.

Nolte, K. 1979. Determination of Fracture Parameters from Fracturing Pressure Decline. SPE-8341-MS Paper Presented at the SPE Annual Technical Conference and Exhibition, 23-26 September, Las Vegas, Nevada. https://doi.org/10.2118/8341-MS.

Singh, P., Agarwal, R., and Krase L. 1987. Systematic Design and Analysis of Step-Rate Tests to Determine Formation Parting Pressure. SPE-16798-MS Paper Presented at the SPE Annual Technical Conference and Exhibition, Dallas, Texas, 27-30 September. https://doi.org/10.2118/16798-MS.

Vermylen, J. 2011. Geomechanical Studies of the Barnett Shale, Texas, USA. Retrieved from https://stacks.stanford.edu/file/druid:zf098jx2047/Vermylen%20Dissertation%20%28Registrar%29-augmented.pdf

Wang, H. and Sharma, M. 2018. Estimating Un-propped Fracture Conductivity and Fracture Compliance from Diagnostic Fracture Injection Estimating Un-propped Fracture Conductivity and Fracture Compliance from Diagnostic Fracture Injection Tests. *SPE Journal* **23**(5): 1648-1668. https://doi.org/10.2118/189844-PA.

Xing, P, Winkler, D., Rickard, B., et al. 2020. Interpretation of In-Situ Injection Measurements at the FORGE Site. Paper Presented at the 45th Workshop on Geothermal Reservoir Engineering at Stanford, California, February 10-12.

Zoback, M. 2007. *Reservoir Geomechanics*. Cambridge: Cambridge University Press. doi:10.1017/CBO9780511586477.

Zoback, M. and Haimson, B. 1982. Status of the Hydraulic Fracturing Method for In-Situ Stress Measurements. ARMA-82-141 Paper Presented at the 23rd U.S Symposium on Rock Mechanics (USRMS), Berkeley, California), 25-27 August.

Zoback, M. and Kohli, A. 2019. *Unconventional Reservoir Geomechanics: Shale Gas, Tight Oil, and Induced Seismicity*. Cambridge: Cambridge University Press. https://doi.org/10.1017/9781316091869.

Zoback, M. and Lund-Snee, J. 2018. Predicted and Observed Shear on Pre-existing Faults during Hydraulic Fracture Stimulation. *SEG Technical Program*: 3588-3592. https://doi.org/10.1190/segam2018-2991018.1.